AD-A070 256 SOUTHWEST RESEARCH INST SAN ANTONIO TEX F/G 11/2
COMPRESSIVE STRENGTH AND INDENTATION DAMAGE IN CERAMIC MATERIAL--ETC(U)
JUN 79 J LANKFORD, D L DAVIDSON N00014-75-C-0668

UNCLASSIFIED NL

| OF |
AD
A070256

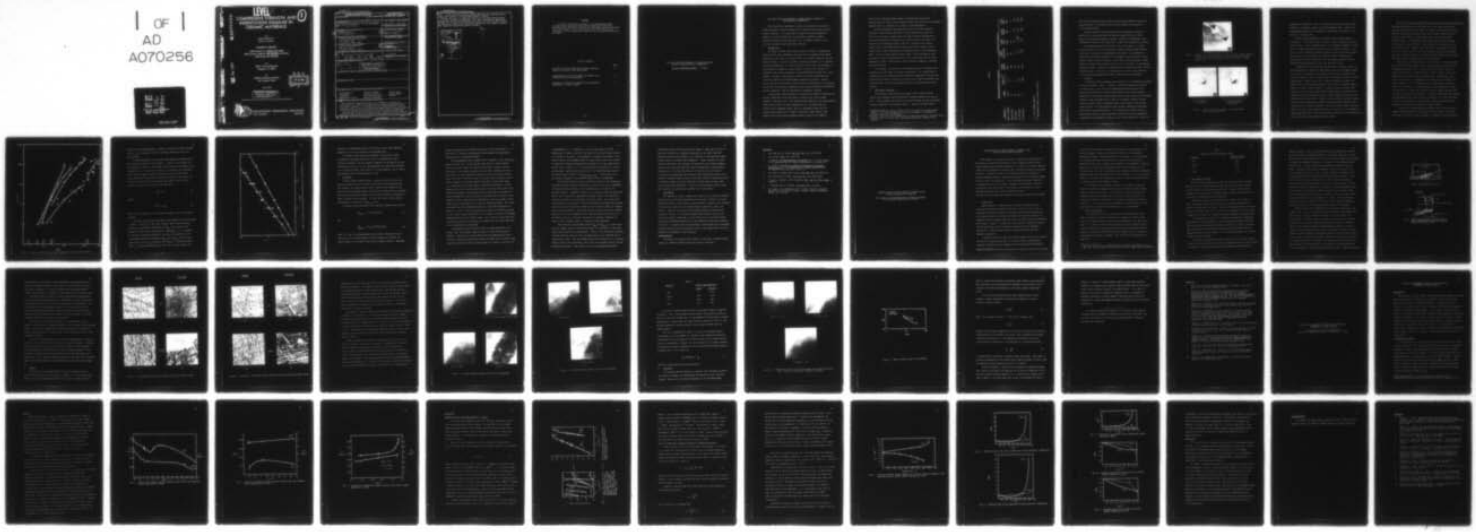

END
DATE
FILMED
7-79
DDC

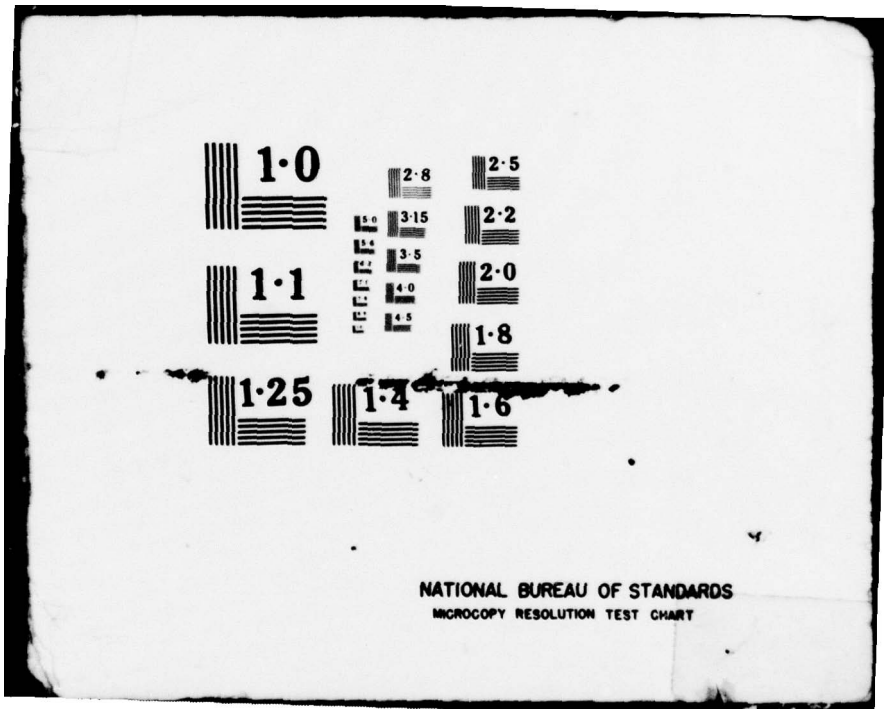
1·0
1·1
1·25
2·8
3·15
3·5
4·0
4·5
1·4
2·5
2·2
2·0
1·8
1·6
NATIONAL BUREAU OF STANDARDS
MICROCOPY RESOLUTION TEST CHART

LEVEL II

COMPRESSIVE STRENGTH AND INDENTATION DAMAGE IN CERAMIC MATERIALS

by
James Lankford, Jr.
David L. Davidson

TECHNICAL REPORT

ONR Contract No. N00014-75-C-0668
ONR Contract Authority NR 032-553/1-3-75(471)
SwRI Project No. 02-4231

for
Office of Naval Research
Arlington, VA 22217

by
Southwest Research Institute
San Antonio, Texas

June 1979

SOUTHWEST RESEARCH INSTITUTE
SAN ANTONIO HOUSTON

Unclassified

SECURITY CLASSIFICATION OF THIS PAGE (When Data Entered)

REPORT DOCUMENTATION PAGE

READ INSTRUCTIONS BEFORE COMPLETING FORM

1. REPORT NUMBER

2. GOVT ACCESSION NO.

3. RECIPIENT'S CATALOG NUMBER

4. TITLE (and Subtitle)
(6) Compressive Strength and Indentation Damage in Ceramic Materials

5. TYPE OF REPORT & PERIOD COVERED
31 May 1978 - 31 May 1979

6. PERFORMING ORG. REPORT NUMBER

7. AUTHOR(s)
(10) James Lankford, Jr.
David L. Davidson

8. CONTRACT OR GRANT NUMBER(s)
(15) N00014-75-C-0668

9. PERFORMING ORGANIZATION NAME AND ADDRESS
Southwest Research Institute
P.O. Drawer 28510
San Antonio, Texas 78284
328 200

10. PROGRAM ELEMENT, PROJECT, TASK AREA & WORK UNIT NUMBERS
NR 032-553/1-3-75 (471)

11. CONTROLLING OFFICE NAME AND ADDRESS
Office of Naval Research
800 North Quincy
Arlington, Virginia 22217

(11) 12. REPORT DATE
June 1979

13. NUMBER OF PAGES

14. MONITORING AGENCY NAME & ADDRESS (if different from Controlling Office)
(9) Technical rept.
31 May 78 - 31 May 79

15. SECURITY CLASS. (of this report)
Unclassified

15a. DECLASSIFICATION/DOWNGRADING SCHEDULE

16. DISTRIBUTION STATEMENT (of this Report)
(12) 53 p.

DISTRIBUTION STATEMENT A
Approved for public release;
Distribution Unlimited

17. DISTRIBUTION STATEMENT (of the abstract entered in Block 20, if different from Report)

18. SUPPLEMENTARY NOTES

19. KEY WORDS (Continue on reverse side if necessary and identify by block number)

Microplasticity	Acoustic Emission	Plastic Zone
Indentation	Cracking Threshold	Surface Damage
Compression	Microcrack Initiation	Ceramics
Temperature Effects	Electron Channeling	

20. ABSTRACT (Continue on reverse side if necessary and identify by block number)

The threshold loads and crack sizes for indentation cracking were investigated for a number of ceramics using scanning electron microscopy and acoustic emission. It was found that the cracking behavior could be predicted, using a fracture mechanics/dimensional analysis approach modified to take into account the stress field at an elastic-plastic indentation.

Selected area electron channeling was used to characterize the extent of subsurface damage produced in ceramics during grinding and polishing opera-

over

DD FORM 1 JAN 73 1473 EDITION OF 1 NOV 65 IS OBSOLETE

328 200

Unclassified

SECURITY CLASSIFICATION OF THIS PAGE (When Data Entered)

tions. It was found that polishing damage depths can be correlated using a simple model based on a sliding elastic-plastic indenter.

Finally, the effect of temperature and strain rate upon material removal and cracking threshold was analyzed, using recent experimental compressive strength and crack growth measurements as inputs to current predictive models. The results are shown to have surprising implications with regard to dynamic, high temperature indentation (particle impact).

FOREWORD

This report describes the results of an experimental program oriented toward correlating compressive strength and microfracture mechanisms with indentation resistance and indentation fracture mechanisms for strong ceramics. Some of the progress made toward this goal is summarized in the following three technical papers (preprints) comprising the report.

TABLE OF CONTENTS

THE CRACK INITIATION THRESHOLD IN CERAMIC MATERIALS SUBJECT TO ELASTIC/PLASTIC INDENTATION

(Journal of Materials Science , In Press)

THE CRACK INITIATION THRESHOLD IN CERAMIC MATERIALS SUBJECT TO ELASTIC/PLASTIC INDENTATION

The threshold for indentation cracking is established for a range of ceramic materials, using the techniques of scanning electron microscopy and acoustic emission. It is found that by taking into account indentation plasticity, current theories may be successfully combined to predict threshold indentation loads and crack sizes. Threshold cracking is seen to relate to radial rather than median cracking.

1. Introduction

The impact of small, hard particles upon the surfaces of engineering ceramics often causes indentation cracking, which can degrade the mechanical properties of the target in two major areas: (1) erosion resistance, and (2) tensile strength. In order to optimize operating performance, it is important to know the parameters, i.e., load, crack size, crack shape, corresponding to the threshold for damage in a given ceramic, as well as the influence of deformation and fracture properties in establishing this threshold for a given ceramic. Currently, there appears to exist no reliable experimental data concerning indentation threshold damage parameters in ceramics. However, recent progress has been made in the theoretical consideration of the influence of both the elastic/plastic indentation stress field, and material deformation/fracture properties, upon the threshold for indentation cracking.

In particular, Lawn and Evans [1] have developed a model to determine the critical conditions for the initiation of cracks at the sites of sharp indenters. The model uses a very simplified approximation to the elastic/plastic stress field field of an actual indentation; i.e., one based upon the solution for an expanding cavity, and as a consequence assumes that the initial cracks formed will be "median" (subsurface, penny-shaped) flaws lying at the elastic/plastic boundary beneath the apex of the indenter.

From a fracture-mechanics-based analysis utilizing this stress field representation, the sizes of the earliest-formed cracks, and their corresponding indenter loads, are predicted for a range of ceramic materials.

Another recent model, developed principally to describe Palmqvist* cracking in tough ceramics like WC-Co, has been proposed by Perrott [2]. In this case, account is taken of the fact that the stress distribution on the indenter/indentation interface is not really constant, but rather is a function of the indentation plastic zone size. Because of this stress redistribution, the maximum tensile field occurs near the surface, at the indent corners, rather than below the indentation apex as in the Lawn-Evans model. Thus the Perrott theory predicts radial, rather than median, crack nucleation. Unlike the Lawn-Evans theory, the Perrott model does not rank materials in terms of their critical crack nucleation parameters, threshold load and crack size.

In this paper, the results of an experimental study of threshold crack nucleation in a wide range of ceramics are described. It is shown that by considering the two existing theoretical models in combination, the materials studied may be ranked successfully in terms of their relative threshold crack sizes and loads; further, both parameters may be predicted with surprising accuracy.

2. Experimental Procedure

The materials chosen consisted of single crystal sodium chloride, silicon, and germanium, and polycrystalline aluminum oxide** and silicon carbide†. These provided a wide range in electronic bonding type and deformation/fracture properties, as indicated in Table 1. Faces of the NaCl crystal

*Palmqvist cracks are shallow, radial surface fractures lying within median planes (i.e., planes containing the axis of the indenter), extending out from the corners of an indentation.

**Lucalox, 25 μm grain size, General Electric Lamp Glass Division, Cleveland, Ohio.

†Sintered α-SiC, 7 μm grain size, Carborundum Corporation, Niagara Falls, New York.

Table 1

Material	Deformation/Fracture Parameters		Threshold Parameters				
	H(GPa)	K_c(MPa $m^{1/2}$	P*(gm) Theory	P*(gm) Theory (corrected)	P*(gm) Exp	c*(μm) Theory	c*(μm) Exp
NaCl (crystal)	0.24	0.5	4000	725	1500	120	100
Al_2O_3 (poly)	12	4	300	26	25	5	3
SiC (poly)	19	4	80	8	10	2.0	1.0
Si (crystal)	10	0.6	0.3	2.5†	5 (3‡)	0.2	0.65
Ge (crystal)	9	0.46	0.15	1.25†	2.0	0.14	0.25

† $\eta = 0.1$ rather than 1.0

‡ Experimental result of Sata, et al [7].

were {100} as-cleaved surfaces, while the silicon and germanium crystals had as-grown surfaces. The Al_2O_3 and SiC specimen surfaces were polished to a 0.25 μm diamond finish.

Acoustic emission (AE) was monitored using an apparatus (described previously [3]) operating within the frequency domain 100 kHz to 1 MHz, using a PZT transducer resonant at 160 kHz. During the microhardness tests, specimens were tested on an alumina base, to which the transducer was affixed.

Microhardness tests were carried out over a load range of 1 to 6000 gm; during each test, the quasi-statically applied, diamond pyramid indenter rested upon the specimen for approximately 18 seconds. The threshold for indentation cracking was determined to correspond to the lowest load at which acoustic emission could be detected. At all loads at which emission occurred, optical or electron microscopy was used to verify the presence of, and measure, indentation cracks. Similarly, the SEM was used to ensure that "quiet" (no AE) indentations were crack-free. For observation in the SEM, it was necessary to coat the Al_2O_3 specimens with a thin, conducting film of palladium.

3. Results

Deformation/fracture phenomena characteristics of the indentation threshold are shown in Figures 1 and 2. In Figure 1, both NaCl indents were produced by 1500 gm loads. Since this is the approximate threshold load for this material, the presence of cracks is very sensitive to the local microflaw population in the vicinity of each indent corner. Thus, only one of the indents displays cracks, and these only at three of the corners; clearly, the only cracks are radial, with no subsurface median cracks visible in this transparent material. In this particular case, acoustic emission was associated only with the cracked indentation. It is interesting to observe that the NaCl formed indentation cracks only when oriented such that the indentation diagonals were approximately parallel to <110>; when rotated 45°, so that the

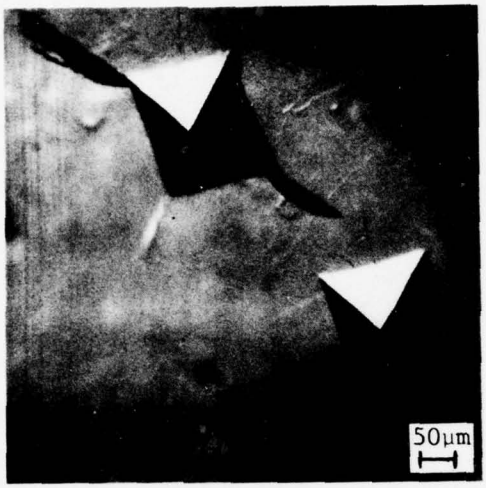

Figure 1. Indents on as-cleaved {100} face of NaCl crystal, indent diagonals parallel to <110>, both indents caused by 1500 gm load, with radial cracks nucleated adjacent to the upper indent, optical view at 55X.

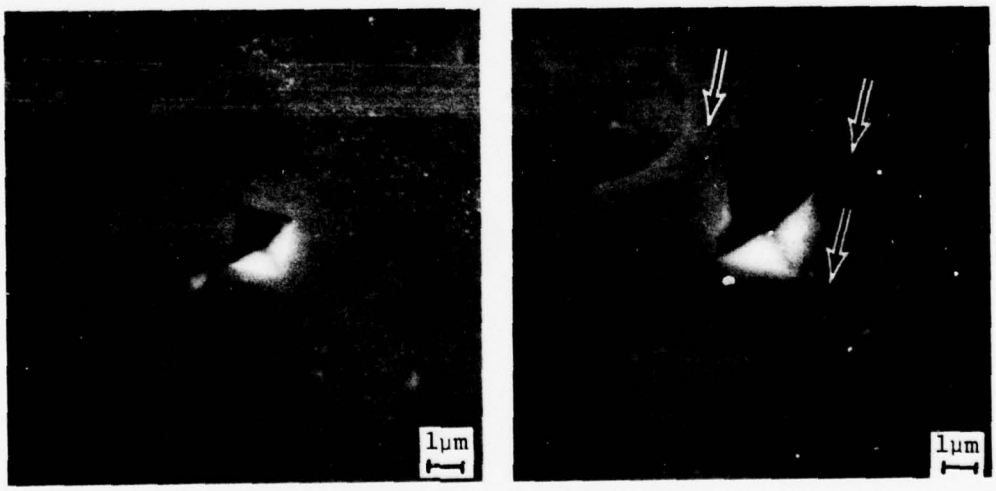

(a) 25 gm load, no cracking

(b) 50 gm load, radial cracking (arrow), twins formed

Figure 2. Indents on polished surface of polycrystalline Al_2O_3, SEM view at 2800X.

diagonals were parallel to <100>, no cracks were obtained for loads as high as 6000 gm, the maximum capacity of the microhardness tester. Similar crystallographic dependencies of indentation cracking have been noted [4] for other ionic solids as well.

The near threshold behavior of aluminum oxide is shown in Figure 2. In Figure 2a, a 25 gm load is seen to produce a perfect indentation, with no visible cracks. Acoustic emission did not occur during the formation of this indent. Cracking and acoustic emission both were detected, however, at the site of the 50 gm indentation shown in Figure 2b, where three radial cracks have nucleated. At loads above the threshold, radial cracking in both materials was observed consistently, with corresponding acoustic emission. Similar behavior was observed in the other materials tested.

Interpretation of the initially observed cracks as radial, rather than the manifestation of subsurface, penny-shaped median cracks breaking through to the surface is important, and is based on the following considerations. First, the cracks in NaCl are clearly radial. Additionally, study of cleaved indentations in single crystal α-SiC (reported elsewhere [8]) shows that radial cracks in this material definitely form in lieu of subsurface median cracks, for loads as high as 3500 gm. Presently unreported results (this laboratory) of serial sectioning through cracked indents in polycrystalline Al_2O_3 show that in this material as well, initial indentation fractures are shallow radial surface cracks. Finally, acoustic emission was never obtained in any of the five materials studied for loads below which apparent radial cracks were first visible in the SEM. Since in the several cases cited above (NaCl, SiC, Al_2O_3) these cracks were proven to be radial, it is reasonable to suppose that those which in Si and Ge likewise appeared only in coincidence with the threshold acoustic emission, also were radial.

The acoustic emission associated with radial cracking occurred predominantly upon immediate application of the load; very little stress wave activity took place during the period in which the indenter rested upon the specimen. Moreover, except for fairly high loads, little acoustic response was seen as the load was removed. In these latter cases, the emission had two possible sources: (1) extension of the radial cracks formed on loading; (2) nucleation of lateral cracks. This point will be the subject of work to be reported later. However, since the counts on unloading constituted such a very small fraction of the total emission (loading plus unloading), the acoustic emission counts to be reported represent those detected within approximately the first half second of load application.

These results are summarized in Figure 3, where P is the quasi-static load, and N the average number of total counts accumulated during a series of indentations at each load. It can be seen that for each ceramic, N decreases with P until a threshold value in load is reached. This point, indicated by the arrows along the horizontal axis, was defined in two ways: For Si and Ge, it corresponds to the load at which cracking, hence acoustic emission, is so infrequent that the average number of emission counts is less than one. On the other hand, it was determined for Al_2O_3, SiC, and NaCl to be simply the load below which no acoustic emission (and no cracks as well) could be detected. It should be emphasized that scanning electron microscopy was used to verify the presence of at least one radial crack at each indentation for which acoustic emission was detected, and conversely, the absence of cracks at all "quiet" indents.

In addition to establishing the threshold load for cracking, which ranges from approximately 2 to 1500 gms, the data of Figure 3 also rank the ceramics in terms of their resistance to indentation crack nucleation.

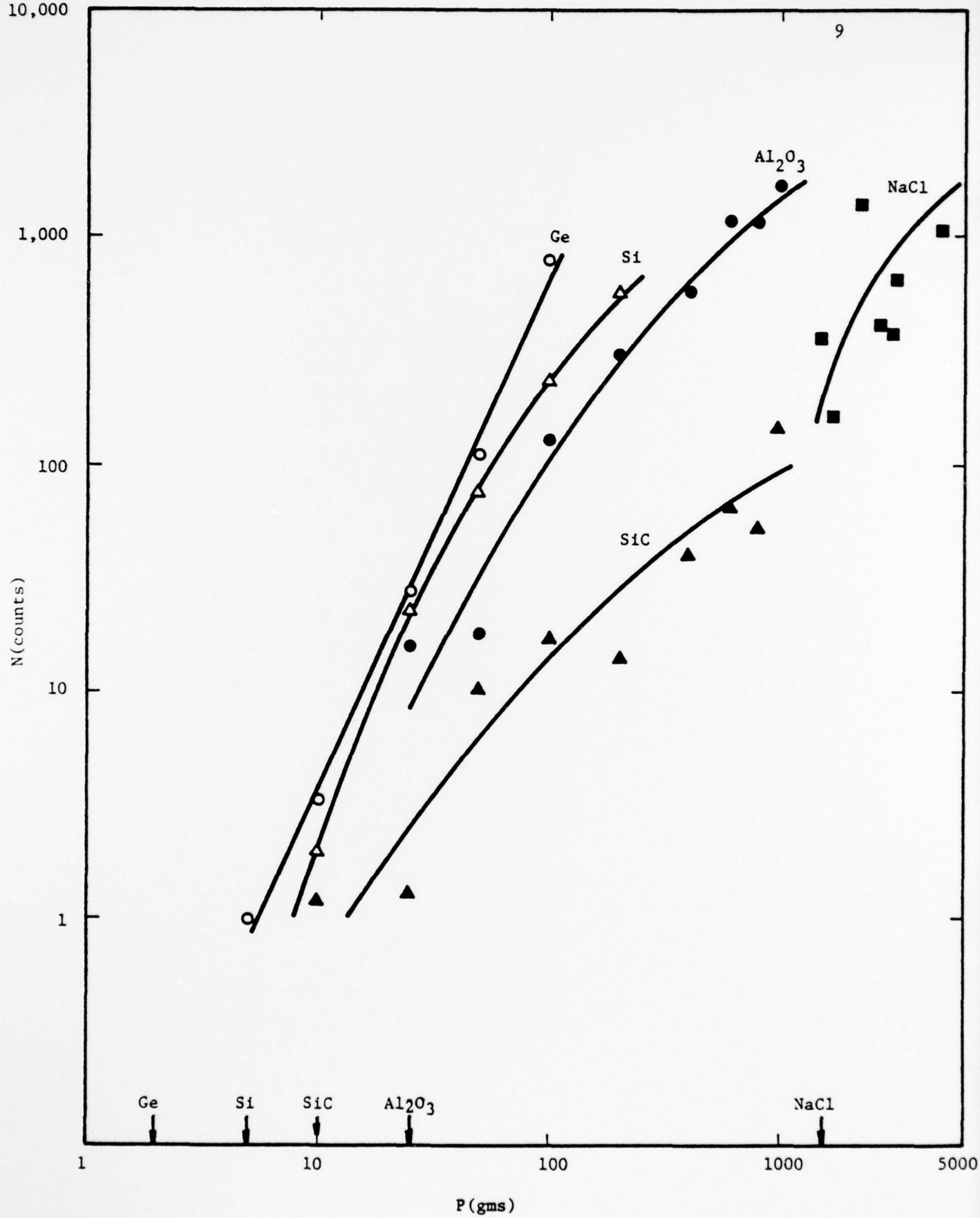

Figure 3. Acoustic Emission Counts Versus Indentation Load for Various Ceramics

The least crack resistant material, insofar as concerns the load to produce a crack, is Ge, followed in order of increasing resistance by Si, SiC, Al_2O_3 and NaCl.

The SEM measurements of crack length and indentation dimension also were plotted, as shown for SiC in Figure 4. There the crack length (2c) is considered to consist of the radial corner cracks plus the length of the indentation (2a). As seen in the figure, this procedure gives remarkably good load/crack length correlation, despite the fact that the corner cracks apparently do not actually penetrate the indent at low loads. For all materials studied, it was found that the indenter load P could be related to a and c over the entire load range by [5]

$$P/a^2 = 2H \tag{1}$$

and [6]

$$P/c^{3/2} = \beta_o K_c \tag{2}$$

where H is the hardness, K_c is the fracture toughness, and β_o an indenter constant.

Threshold crack nucleation parameters are summarized for each material in Table I. Here P^*_{Exp} is the lowest indenter load for which cracking occurred, as determined by SEM and AE, and C^*_{Exp} is the length of the individual radial cracks corresponding to these P^*_{Exp}'s; i.e., excluding the uncracked indentation dimension. Included for comparison are the corresponding theoretical parameters P^*_{Theory} and c^*_{Theory} from the Lawn-Evans theory, with c^*_{Theory} defined as the radius of a subsurface median crack. The relationship between the latter and a surface radial crack

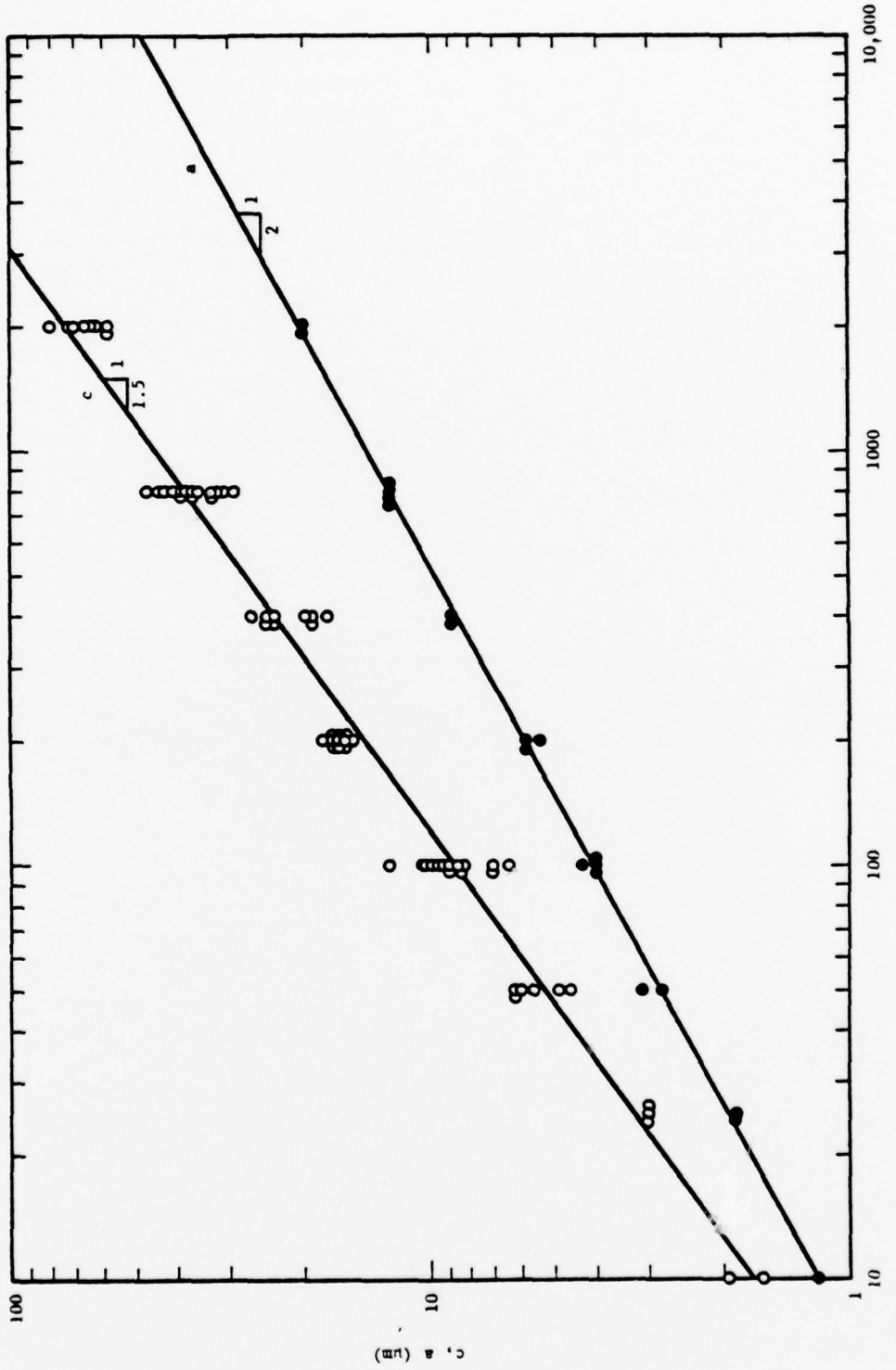

Figure 4. Crack Length and Indentation Dimension Versus Indentation Load for Polycrystalline SiC

attached to an indentation corner is not obvious, so the crack dimension comparison in this case can only be an approximate one.

It should be noted that to the knowledge of the authors, almost no comparable experiments have been carried out regarding the crack nucleation threshold. The only apparent comparison is afforded by the very limited work of Sata, et al. [7], who determined the indentation threshold in Si using replica TEM. They found P^* to be approximately 3 gm, in fairly good agreement with the present value of 5 gm.

4. Discussion

From the results reported above, it seems clear that in all of the materials studied, the first cracks to form, hence those associated with the threshold, are radial surface cracks. Moreover the ordering of the materials by the Lawn-Evans theory is perfect with respect both to threshold load level and crack size, despite the fact that the theory is intended to apply to median crack nucleation. *It is for this latter reason, however,* that numerical inaccuracies in P^*_{Theory} arise.

According to Lawn and Evans [1] the threshold parameters are given by

$$c^*_{Theory} = (1.767/\theta^2)(K_c/H)^2 \tag{3}$$

and

$$P^*_{Theory} = (54.47\alpha/\eta^2\theta^4)(K_c/H)^3 K_c \tag{4}$$

where θ, η, and α are dimensionless factors related respectively to the peak stress at the elastic-plastic boundary beneath the indenter, the spacial extent of the tensile field, and the indenter geometry. Agreement

between the predicted and observed crack sizes is quite good (Table I). In the case of P^*, however, the predicted values disagree with experimental observations by a considerable margin.

This disagreement can be rationalized by appealing to the theoretical model of Perrott [2]. We have already shown that the cracks nucleated in this study were radial, as required by the model. However, rigorous application of this analysis requires that two other conditions be met as well, namely (1) that considerable subsurface plasticity must be present, and (2) in order for the hoop stress in the near-surface region to achieve tensile character, the surface plastic zone must be sufficiently large, i.e., approximately 50% larger than the indentation impression. We have addressed the first of these qualifications for the particular case of SiC, using a new technique (selected area electron channeling) as described in detail elsewhere [8], with the principal conclusion that the extent of the subsurface plastic zone beneath an indentation in silicon carbide is quite large, equal to approximately five times the impression radius. The second requirement has been established through the recent TEM observations of Hockey, et al [9], in which the near-surface plastic zone radius was found, for SiC, Al_2O_3, and MgO (hence NaCl), to be clearly in excess of the minimum dimension required by the Perrott theory. For Si and Ge, it was found that near-surface plasticity was present at distances from the indent which were in the neighborhood of the minimum.

Assuming,then, that the Perrott model is indeed applicable in the present case, the threshold loads calculated by Lawn and Evans must be modified. Specifically, Perrott showed that the maximum tensile stress across the subsurface median plane beneath the indent apex is actually lower than that acting across surface radial planes by a factor of $(1-2\nu)/(7-2\nu)$,

or approximately 13. In addition, it is clear that based on the TEM observations of Hockey, et al [9], the value of $\eta(=1)$ used by Lawn and Evans is too large for Si and Ge. This parameter is related to the extent of the surface tensile field embedded within the near-surface plastic zone created by compressive stresses; considering the minimal size of their observed [8] surface zones, a value of $\eta \simeq 0.1$ would appear more appropriate for silicon and germanium. Applying these corrections to the Lawn-Evans data produces the results shown in Table I as $P^*_{Theory(Corrected)}$. In this case, quite satisfactory agreement is now obtained between theory and experiment.

These results indicate that the Lawn-Evans approach to the indentation threshold cracking problem is essentially correct, but errs in its assumption of subsurface median cracking as the threshold event (at least for the materials studied). Basically, instead of a situation in which the subsurface plastic zone "searches" for subsurface nucleation centers, one envisions a near-surface plastic zone "searching" for surface flaws. This arises from the unexpectedly large degree of plasticity apparently associated with indentations in even such strong, hard ceramics as SiC, and which alters the indentation stress distribution to the extent that the Perrott model must be invoked. However, the critical dependence of the cracking threshold upon H and K_c is not thereby affected, so that the (qualitative) ordering of materials in terms of their threshold loads for cracking is valid regardless.

Considering the good agreement between c^*_{Exp} and c^*_{Theory}, it seems clear that the cracks created at the threshold should be considered to be the small radial ones attached to the indentations. However, from the fracture mechanics-lifetime prediction point of view, the flaw created at the threshold may be significantly larger. The flaw probably should be considered to be a continuous shallow surface crack consisting of the radial crack segments plus the central, uncracked indentation. This is borne out by the experimentally obtained

relationship between load and total crack length 2c summarized in Figure 4. Since the threshold for cracking is determined by the lowest loads and smallest cracks plotted in Figure 4, the remainder of the load-crack length results should be concerned with propagation. Indeed, Equation (2), which describes these data, has precisely the same form as the fracture mechanics equation for equilibrium penny-like cracks extending under center-loading conditions [6]. The fact that there is no break in plots like Figure 4 as loads are increased above the threshold value thus implies that the very smallest indentation-induced flaws, although well within the indentation field of influence, behave like large flaws whose cracked region is much larger than the nucleating indentation. From the fracture mechanics point of view, they therefore are analytically treatable in the same fashion.

5. Conclusions

The ordering of various ceramics with regard to their relative threshold loads and crack sizes during indentation microfracture is shown to be accomplished successfully by the theory of Lawn and Evans, although at the threshold, radial surface, rather than the predicted median subsurface, cracks, are observed. Moreover, the sizes of the threshold cracks are predicted with reasonable accuracy. The cracking threshold load, however, is in error by more than an order of magnitude, a factor which can be corrected by taking into account indentation plasticity and the indentation stress field analysis of Perrott. It appears that fracture mechanics relationships may be applicable without alteration from the macroscopic surface crack regime down to the very threshold for indentation crack nucleation.

Acknowledgement

The authors are grateful for the support of the Office of Naval Research, Contract No. N00014-75-C-0668, during the course of this work.

References

1. B.R. Lawn and A.G. Evans, Jour. Mat. Sci., 12, (1977) 2195.

2. C.M. Perrott, Wear, 45, (1977) 293.

3. J. Lankford, Fracture Mechanics of Ceramics, Vol. 3, ed. R.C. Bradt, D.P.H. Hasselman, and F.F. Lange, Plenum Press, N.Y., (1978) 245.

4. B.J. Hockey, The Science of Hardness Testing and its Research Applications, ed. J.H. Westbrook and H. Conrad, American Society for Metals, Metals Park, Ohio, (1973) 30.

5. B.R. Lawn, T. Jensen, and A. Arora, Jour. Mat. Sci., 11 (1976) 575.

6. B.R. Lawn and E.R. Fuller, Jour. Mat. Sci., 10, (1975) 2016.

7. T. Sata, K. Takamoto, and H. Yoshikawa, Bull. Jap. Soc. Prec. Engg., 3, (1969) 13.

8. J. Lankford and D.L. Davidson, Jour. Mat. Sci. (in press).

9. B.J. Hockey, S.M. Weiderhorn, and H. Johnson, "Erosion of Brittle Materials by Solid Particle Impact," National Bureau of Standards NBSIR, (1977) 77-1396.

CHARACTERIZATION OF SURFACE DAMAGE IN CERAMICS USING
SELECTED AREA ELECTRON CHANNELING

(The Science of Ceramic Machining and Surface Finishing,
II, NBS Special Publication, In Press)

CHARACTERIZATION OF SURFACE DAMAGE IN CERAMICS USING SELECTED AREA ELECTRON CHANNELING

The technique of selected area electron channeling has been applied to the problem of characterizing subsurface plastic damage introduced during ceramic machining and polishing operations. The surfaces of ceramics spanning a wide range in hardness were prepared under controlled grinding and polishing conditions. Subsurface regions of sectioned specimens were subjected to electron channeling analysis, enabling the boundaries of the subsurface damage (plastic) zones to be mapped out. It was determined that under conditions of constant applied load, the depth of damage during polishing is inversely proportional to the square root of the hardness; this finding is in good agreement with predictions based on indentation theory.

Key Words: Electron channeling; plasticity; subsurface damage; surface damage.

1. Introduction

Damage produced in ceramic materials through conventional surface preparation techniques can manifest itself in at least two ways. First, a population of microflaws capable of degrading the mechanical properties may be introduced; Becher, for example, has shown [1][1] that twins generated in alumina by surface grinding constitute failure initiation sites upon subsequent bend testing. Second, it is known that microplasticity attending mechanical surface preparation can be reflected in significant surface compressive stresses [2]. These likewise can exert an appreciable influence upon mechanical properties.

A consistent problem in dealing with these damage factors is the inherent difficulty in characterizing them. To a certain extent, topographically sensitive techniques such as scanning electron microscopy and profilometry

[1]Figures in brackets indicate the literature references at the end of this paper.

can be used to characterize features such as surface cracks, pullouts, and surface roughness. However, the depth and severity of near subsurface microplastic damage is much more difficult to ascertain. In a few materials such as MgO, dislocation etch-pitting can be used to accurately map the subsurface plastic zone. However, the technique is not applicable in general, especially for materials of engineering interest such as Al_2O_3, SiC, etc. In these latter cases the only available data regarding the depth of machining damage have come from TEM studies such as those of Hockey, et al. [3,4], which because of the difficulty in knowing precisely the depth from which the foils are taken, provide rough estimates at best.

In this paper, a new technique is shown to be capable of providing hitherto unavailable information concerning near subsurface plastic damage layers in engineering ceramics. The technique of selected area electron channeling has been used primarily in the study of metal plasticity, but was recently applied by the authors to the study of indentation plasticity in SiC [5]. It is possible that the technique will prove helpful in other applications of ceramics where microplasticity is a consideration.

2. Choice of Materials

The principal criteria for the selection of materials were a wide range in hardness, and that each material be available in single crystal form. The ceramics chosen, and their measured hardnesses, are indicated in Table 1.[2] It was felt that statistical scatter could be reduced by using single crystals, since varying polycrystalline grain orientations would be expected to produce a non-uniform subsurface damage profile, reflecting crystallographic anisotropy in hardness. All crystals were approximately the same size.

---

[2] MgO, with a hardness of ~3.5 GNm^{-2}, was also selected, but chipping of the taper edge during preparation unfortunately precluded damage depth measurements.

Table 1

Materials Chosen and Hardness Values

Material	Hardness (GNm^{-2})
SiC	34.0
Al_2O_3	20.4
Si	11.0
GaAs	7.8

3. Experimental Procedure

For the surface finishing operations, two crystals of every specimen material were each mounted separately upon stainless steel right circular cylinders whose faces had been ground parallel. One set of four mounted specimens was then selected for diamond surface grinding, while the other set was used for metallographic surface polishing.

Grinding was carried out by gripping each cylinder in the chuck of a lathe, and making a pass across the face of the exposed specimen with an 800 grit, diamond bonded cup wheel. The three inch diameter wheel was turned at 3500 rpm, using a feed rate of 25μm/sec and a 25μm depth of cut; a steady stream of water soluble oil coolant was applied throughout the grinding pass.

For polishing, the other set of specimens was mounted in an automatic metallographic polishing apparatus. Wet polishing was performed using 600 grit SiC polishing compound and a pressure of about five pounds. Polishing was continued until an equilibrium situation was achieved with respect to apparent (optical) surface finish, i.e., with further polishing, no change in surface texture was evident.

Following characterization of these surfaces in the scanning electron microscope (using palladium to coat the non-conducting Al_2O_3), it was necessary to section the specimens to allow electron channeling characterization of

subsurface damage. Since it was anticipated that the damage depth probably was not very deep, it appeared desirable to section the specimens on a taper. This "magnifies" depth inversely as the sine of the taper angle, thus increasing the damage zone dimension relative to the diameter of the probing scanning electron beam. The taper sectioning was performed as shown in Figure 1. First, a cylindrical epoxy mount is machined so that one face (A-A') lies 15^{o} from normal to the axis. Next, a ceramic specimen is cemented to this inclined surface with the ground/polished surface facing the mount. These are then placed in a mold, and epoxy is added to reform the cylindrical mount, sealing the specimen within. The mount is sectioned down to B-B' by sequential polishing, taking care to intersect the machined/polished surface of the ceramic, and finally the damage introduced into the ceramic along B-B' during sectioning is removed by ion milling. This process was carried out at the National Bureau of Standards by B. Hockey. Each specimen was argon-ion milled for a minimum of ten hours, so that flaw-free channeling patterns were produced in unground/unpolished areas of the specimens.

Selected area electron channeling has been applied extensively by the authors in the study of localized plasticity in metals [6] and ceramics [5]. The technique, generally described elsewhere [7], is as follows: The electron beam of an SEM is made to rock about a small area on the specimen surface, and the electrons backscattered from that surface are collected. Since electron backscattering is crystallographically specific, a pattern related to the orientation of the crystal is obtained. The acuity of lines within the pattern depends on instrument parameters and on the defect state of the crystal. As the defect density increases, the acuity of the lines on the channeling pattern is decreased. The sensitivity of the line acuity to defect density is material specific, but generally it has been found that very small amounts of crystallite damage may be detected. Suitable theoretical

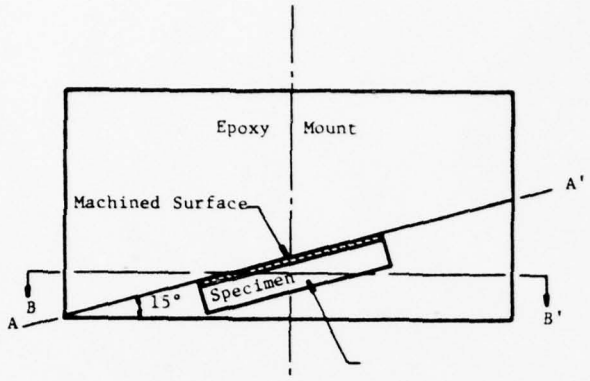

Figure 1. Mounting scheme for taper section

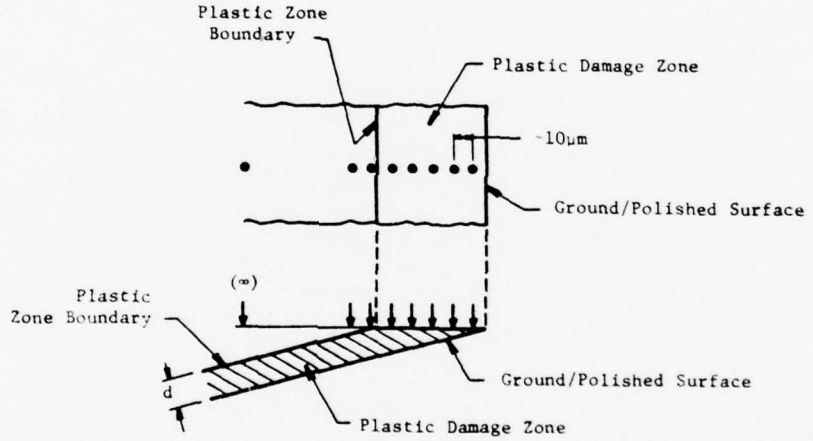

Figure 2. Scheme for determining depth of subsurface plastic zone; arrows and spots indicate locations at which channeling patterns are taken; spot size ~10μm

and experimental techniques are not now available to make quantification of this effect generally possible. Thus, while it is not difficult to define the extent of plasticity, a suitable technique has not been developed to quantify the magnitude of the plasticity determined, except in general terms.

The depth within the crystal from which information is being derived by the channeling technique depends on a combination of materials properties, accelerating voltage of the electron beam and detector characteristics. For the present work, an accelerating voltage of 20 keV was used for all the specimens and instrument parameters yielding a pattern of four degrees were obtained from an approximately 10μm diameter area of the surface. The same instrument parameters were used for all materials.

Since Al_2O_3 is an excellent insulator, it was necessary to vacuum deposit a very thin layer of amorphous graphite on the surfaces of the specimens studied. By carefully controlling the coating thickness, it is possible to obtain channeling patterns from Al_2O_3 which have the same line acuity as from conducting specimens.

The electron channeling data in the present circumstances were obtained from the ion-milled taper-section specimens as sketched in Figure 2. Starting near the machined surface, a local region on the order of 10μm in diameter was interrogated by the electron beam, yielding a channeling pattern. This process was repeated as the beam was moved to other locations further from the surface, until a pattern of identical quality to that found at an "infinite" (large) distance was obtained, thus establishing the depth of plastic damage, d_p.

4. Results

SEM views of the ground and polished surfaces are shown in Figure 3, where hardness decreases moving from top to bottom. It is clear that despite the fact that both grinding and polishing were carried out under identical

GROUND

POLISHED

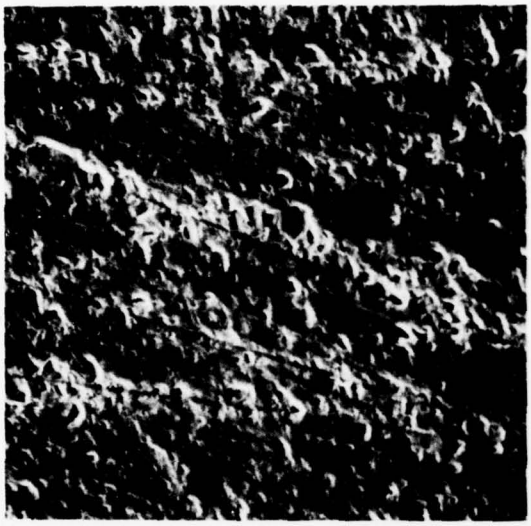

SiC

(a)

(c)

Al_2O_3

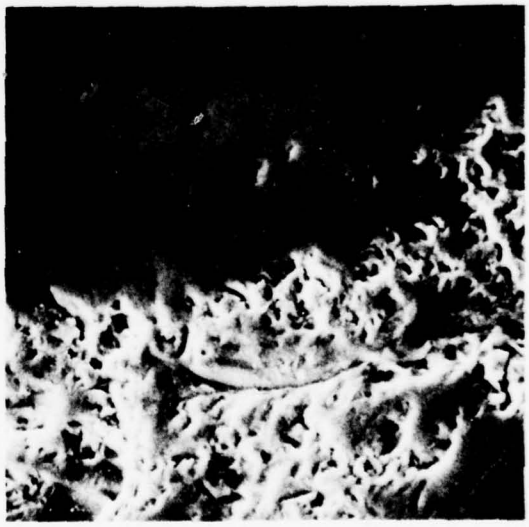

(b)

(d)

FIGURE 3. High magnification views of ground and polished surfaces (700X).

GROUND

POLISHED

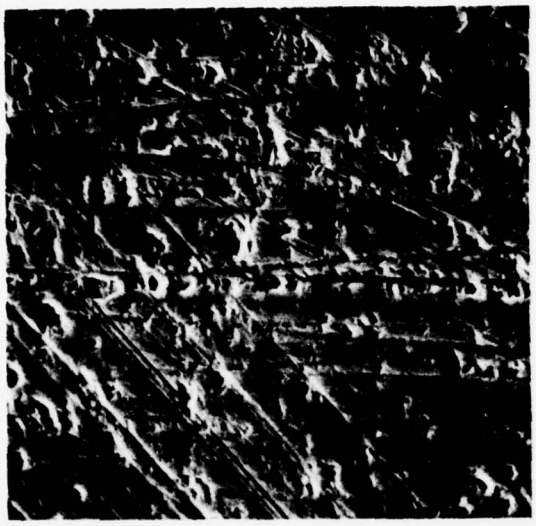

Si

(e)

(g)

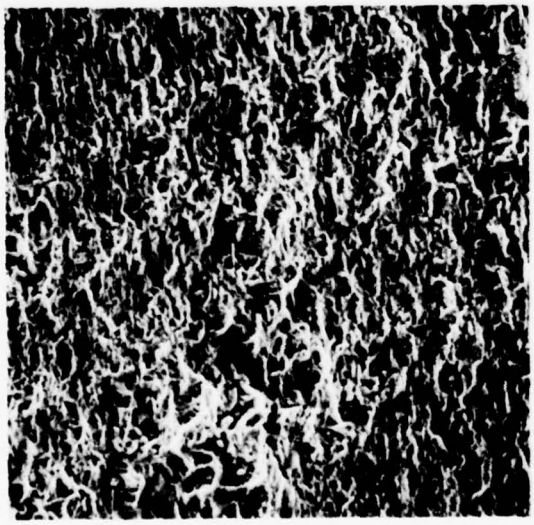

GaAs

(f)

(h)

FIGURE 3. (Continued). High Magnification views of ground and polished surfaces (700X).

conditions for all four materials, there is no correlation between surface features and hardness. For example, ground SiC and Si exhibit chipping along with considerable plastic scoring, while ground Al_2O and GaAs seem to be chipped and burnished. Polished alumina (Fig. 3d) has an extremely smooth surface interspersed with microspalling, while harder SiC (Fig. 3c) and softer GaAs (Fig. 3h) are heavily scored by plastic gouges. In this case, surface appearance is obviously a poor parameter by which to rank ceramics with regard to abrasion resistance.

An example of subsurface damage characterization using electron channeling is shown for GaAs in Figure 4. Five microns beneath the surface, damage is sufficiently extensive that the corresponding channeling pattern is nearly destroyed (Fig. 4a). Somewhat deeper (d = 12μm, Fig. 4b), the pattern begins to emerge, and is quite recognizable just inside the plastic zone (d = 32μm, Fig. 4c). The difference between patterns obtained from just inside, versus anywhere outside, the plastic zone can be clearly discerned by comparing Figures 4c and 4d.

Similar results were obtained for harder materials such as SiC, for which the extent of plasticity is confined to a region nearer the surface. (Table 2 summarizes the damage zone results for all four materials.) Figure 5a shows a distorted pattern 10μm below the surface, and Figure 5b a much clearer version of the same pattern obtained right at the apparent plastic zone boundary. Close comparison between the latter photomicrograph and that corresponding to d = 35μm (Fig. 5c) show that a subtle but resolvable loss in clarity and fineness of detail characterizes the d = 20μm pattern.

(a) d = 5μm

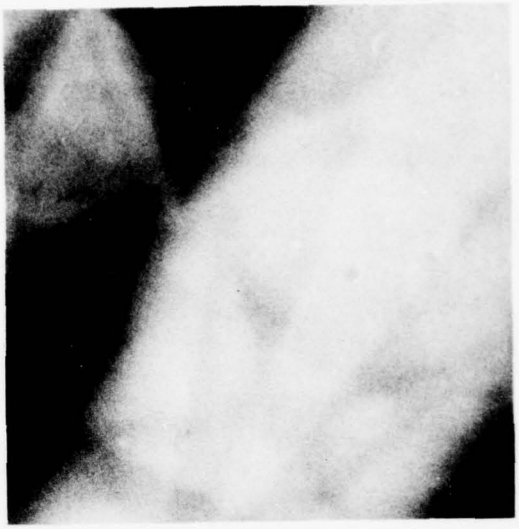

(c) d = 32μm (just inside plastic zone)

(b) d = 12μm

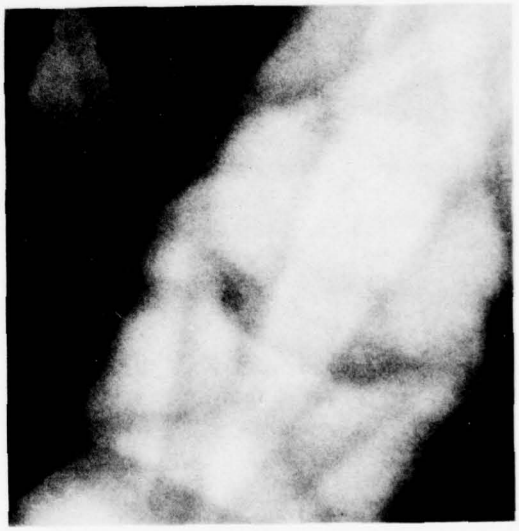

(d) d = ∞

FIGURE 4. Typical channeling pattern results for polished GaAs

(a) d = 10μm

(b) d = 20μm (plastic zone boundary)

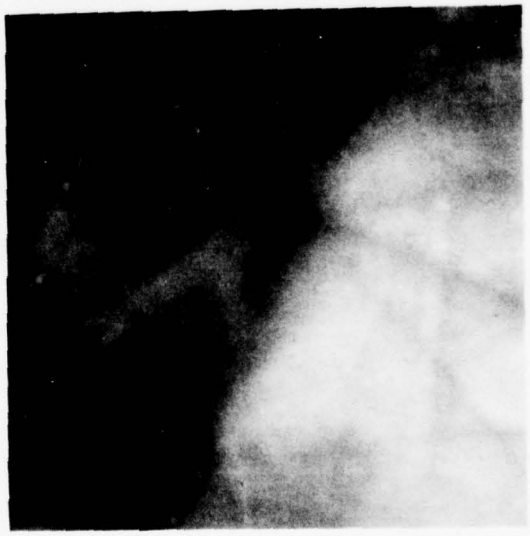

(c) d = 35μm

FIGURE 5. Typical Channeling pattern results for polished SiC

Table 2

Material	Plastic Zone Depth (μm)	
	Ground	Polished
SiC	--	19.5
Al_2O_3	32.0	21.0
Si	32.0	30.4
GaAs	46.5	38.5

The effect of hardness upon the depth of equivalent damage is suggested in Figure 6. At d = 3μm, polished silicon exhibits the pattern of Figure 6a, and at d = 9μm, that of Figure 6b. At approximately the latter depth, polished GaAs produces a pattern (Fig. 6c) lower in quality than that of Si at d = 3μm. The lower hardness of the GaAs clearly exerts a major influence upon the damage gradient.

This fact is emphasized in Figure 7, a plot of the apparent plastic zone boundary d_p versus hardness H. Chipping of the specimen disallowed the determination of d_p for ground SiC, so that the slope of the ground specimen results is questionable. However, for the polished state, it seems reasonable to consider the potential significance of the observed relationship between d_p (polished) and H. As it turns out,

$$d_p \text{ (polished)} \propto \frac{1}{H^{\frac{1}{2}}} \qquad (1)$$

which has interesting theoretical implications.

5. Discussion

The preceding results indicate, as expected, that polishing introduces less subsurface damage, for approximately equivalent grit size, than does grinding. Moreover, the functional dependence of the polishing damage

(a) Si, d = 3μm

(b) Si, d = 9μm

(c) GaAs, d = 8μm

FIGURE 6. Comparison of effect of polishing damage upon channeling patterns for Si and GaAs, showing the influence of hardness.

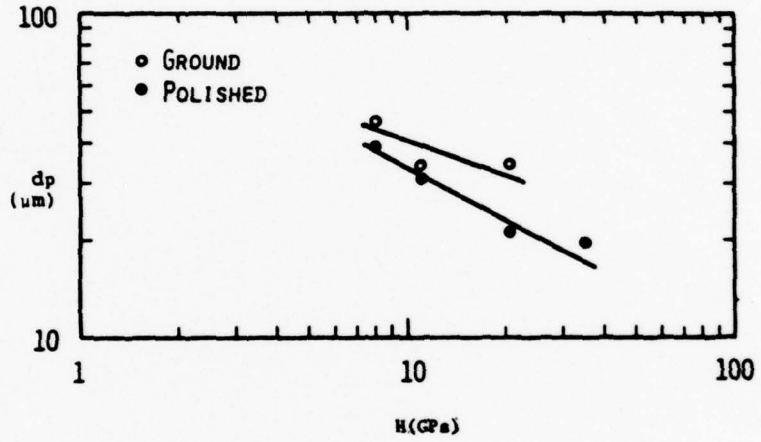

Figure 7. Depth of plastic zone versus hardness.

depth is controlled principally by hardness (under constant load conditions). This observation can be rationalized by appealing to the results of recent studies of the physics and mechanics of the elastic-plastic indentation proces.

It is by now well known [8] that a sharp indenter under a load P produces a plastic impression of characteristic dimension a, which is related to hardness through

$$a = \frac{P^{\frac{1}{2}}}{\alpha \pi H} \tag{2}$$

where α is a geometric constant. If the load is constant, then

$$a \propto \frac{1}{H^{\frac{1}{2}}} \tag{3}$$

Recently, Lawn and Evans suggested [9] on the basis of geometrical similitude considerations that the depth of the plastic zone d_i beneath such an indent should be proportional to a. This prediction was borne out for SiC by recent work by the authors [5]. From equation (2), one would then expect

$$d_i \propto \frac{1}{H^{\frac{1}{2}}} \tag{4}$$

for indentations in materials of varying H under equal loads. This result is predicted independently by the recent elastic-plastic analysis of Perrott [10]. The similarity between equations (1) and (4) is obvious.

From the preceding, it appears that the depth of the subsurface damage zone caused by polishing can be predicted on the basis of indentation theory, whereby a dynamic (sliding) indenter (i.e., a grit particle) behaves like a static indenter. This would imply that if one could determine the depth of

damage in a ceramic of a given hardness subject to prescribed polishing conditions, the damage zone in another ceramic polished under the same conditions could be predicted, based on its hardness alone. It is clear, in addition, that electron channeling recommends itself as a technique for obtaining information on plastic damage in materials which do not lend themselves to conventional damage assessment techniques (such as dislocation etchpitting).

The authors appreciate the support of the Office of Naval Research through Contract No. N00014-75-C-0668 during the course of this work. We are also very grateful for the kind help of Bernard Hockey at NBS, who performed the ion milling.

References

1. Becher, P.F., Fracture-strength anisotropy of sapphire, Jour. Am. Cer. Soc., 59, [1-2], 59-61 (Jan-Feb. 1976).

2. Rice, R.W., Panel discussion (Proc. Symposium Science of Ceramic Machining and Surface Finishing, National Bureau of Standards, Gaithersburg, Maryland, (Nov. 2-4, 1970), Book, The Science of Ceramic Machining and Surface Finishing, NBS Spec. Pub. 348, S.J. Schneider, Jr., and R.W. Rice, eds., pp 407-408 (National Bureau of Standards, Gaithersburg, Maryland, 1972).

3. Hockey, B.J., and Lawn, B. R., Electron microscopy of microcracking about indentations in aluminum oxide and silicon carbide, Jour. Mat. Sci., 10, [8], 1275-1284 (August 1975).

4. Hockey, B.J., Wiederhorn, S.M., and Johnson, H., Erosion of brittle materials by solid particle impact (Proc. 2nd, Int. Conf. Frac. Mech. Ceramics, Pennsylvania State University, State College, Pennsylvania, July 27-29, 1977), Book, Fracture Mechanics of Ceramics, Vol. 3, R.C. Bradt, D.P.H. Hasselman, and F.F. Lange, eds., pp 379-401 (Plenum Press, New York, NY, 1978).

5. Lankford, J., and Davidson, D.L., Indentation plasticity and microfracture in silicon carbide, Jour. Mat. Sci. (in press).

6. Davidson, D.L. and Lankford, J., Plastic strain distribution at the tips of propagating fatigue cracks, Jour. Eng. Mat. and Tech., 98, [1], 24-29 (Jan 1976).

7. Booker, G.R., Scanning electron microscopy-applications (electron channeling effects) in Modern Diffraction and Imaging Techniques in Materials Science, S. Amerlinckx, R. Gevers, G. Remant, and J. van Landuyt, eds., pp 4970653 (North Holland, Amsterdam, 1970).

8. Lawn, B.R., Jensen, T., and Arora, A., Brittleness as an indentation size effect, Jour. Mat. Sci., 11, [3], 573-575 (March 1976).

9. Lawn, B.R., and Evans, A.G., A model for crack initiation in elastic/plastic indentation fields, Jour. Mat. Sci., 12, [11], 2195-2199 (Nov 1977).

10. Perrott, C.M., Elastic-plastic indentation: hardness and fracture, Wear 45, [3], 293-309 (Dec. 1977).

THE EFFECT OF COMPRESSIVE STRENGTH ON THE MECHANICAL PERFORMANCE OF STRONG CERAMICS

(Proceedings of the Third International Conference on Mechanical Behavior of Materials, In Press)

THE EFFECT OF COMPRESSIVE STRENGTH ON THE MECHANICAL PERFORMANCE OF STRONG CERAMICS

INTRODUCTION

Most studies of ceramic strength have emphasized tensile modes of loading, since these materials are especially susceptible to failure under tension. However, certain aspects of mechanical behavior, including even tensile failure, can be controlled or at least influenced significantly by compressive strength or compression-induced damage. In this paper, recent experiments aimed at determining the compressive strength and damage behavior of two strong ceramics are summarized. The results are then considered in terms of current knowledge of lifetime prediction under tensile loading, for material which has suffered prior compressive loads (such as might occur in preloading of ceramic turbine components), and also in terms of current models of indentation/particle impact cracking, as a function of temperature and strain rate (i.e., loading rate).

EXPERIMENTAL PROCEDURES

The compression test setup and procedures have been described in detail elsewhere (Lankford, 1977), and are described here only briefly. Cylindrical specimens of Lucalox[1] Al_2O_3 and sintered α-SiC[2] were compressed at strain rates ranging from 7×10^{-6} to $2 \times 10^{3} sec^{-1}$, the latter achieved by means of the Hopkinson pressure bar; temperatures varied from $-200^{o}C$ to $1600^{o}C$. Acoustic emission (AE) was monitored within the frequency domain 100 kHz to 1 MHz, using a transducer resonant at 160 kHz. Scanning electron microscopy was used to characterize damage induced by loading specimens above the damage threshold established through AE (σ_{AE}).

[1]Type GW, General Electric Lamp Glass Division, Cleveland, Ohio
[2]Carborundum Company, Research and Development Division, Niagara Falls, NY

RESULTS

Compressive strength of Al_2O as a function of temperature is shown in Fig. 1 for a strain rate of $7 \times 10^{-5} sec^{-1}$; also shown is σ_{AE}. The strength generally decreases with temperature, a trend modified by a peak at 350°C, which has previously (Lankford, 1978) been identified with twinning effects. Damage commences at stress levels on the order of $0.5\sigma_f$, consisting of twinning and more importantly, twin-nucleated cracking. For α-SiC, on the other hand, strength at the same $\dot{\varepsilon}$ increases monotonically with temperature as shown in Fig. 2 while σ_{AE} peaks at room temperature. For low temperatures (hence high strain rates), σ_{AE} is very low; in fact, it barely exceeds the tensile strength (Kraft and Dooher, 1976). Damage at this level is typified by short (~10-20μm) cracks.

As a function of strain rate, the room temperature compressive strengths for both Al_2O_3 and SiC increase monotonically (Fig. 3). However, near the upper end of the strain rate range, the strength for SiC undergoes a dramatic increase, nearly doubling within less than two decades in $\dot{\varepsilon}$.

Plotted in Figs. 1-3 as co-functional with σ_f is an empirically established hardness "H", which is scaled based on room temperature, quasi-static hardness measurements. The assumed proportionality between "H" and σ_f over a range in thermally activated states (T, $\dot{\varepsilon}$) is based on empirical evidence, as summarized by Rice (1970), that the yield stress (microhardness/3) is the upper limit of both ambient and elevated temperature compressive strengths. It should be noted that at 23°C, the hardnesses of the Al_2O_3 and SiC are 17 and 24 GNm^{-2}, respectively, in proportional agreement with their corresponding slow strain rate compressive strengths of 3000 and 3800 MNm^{-2} ($\simeq H/6$). Hardness tests over the T-$\dot{\varepsilon}$ range of interest would be extremely difficult to perform, with the adopted procedure, i.e., assuming "$H(T,\dot{\varepsilon})$" $\propto \sigma_f(T, \dot{\varepsilon})$ representing a current best approximation to the actual $H(T, \dot{\varepsilon})$ (note that in Fig. 3, "H" was normalized to σ_f using the Al_2O_3 values).

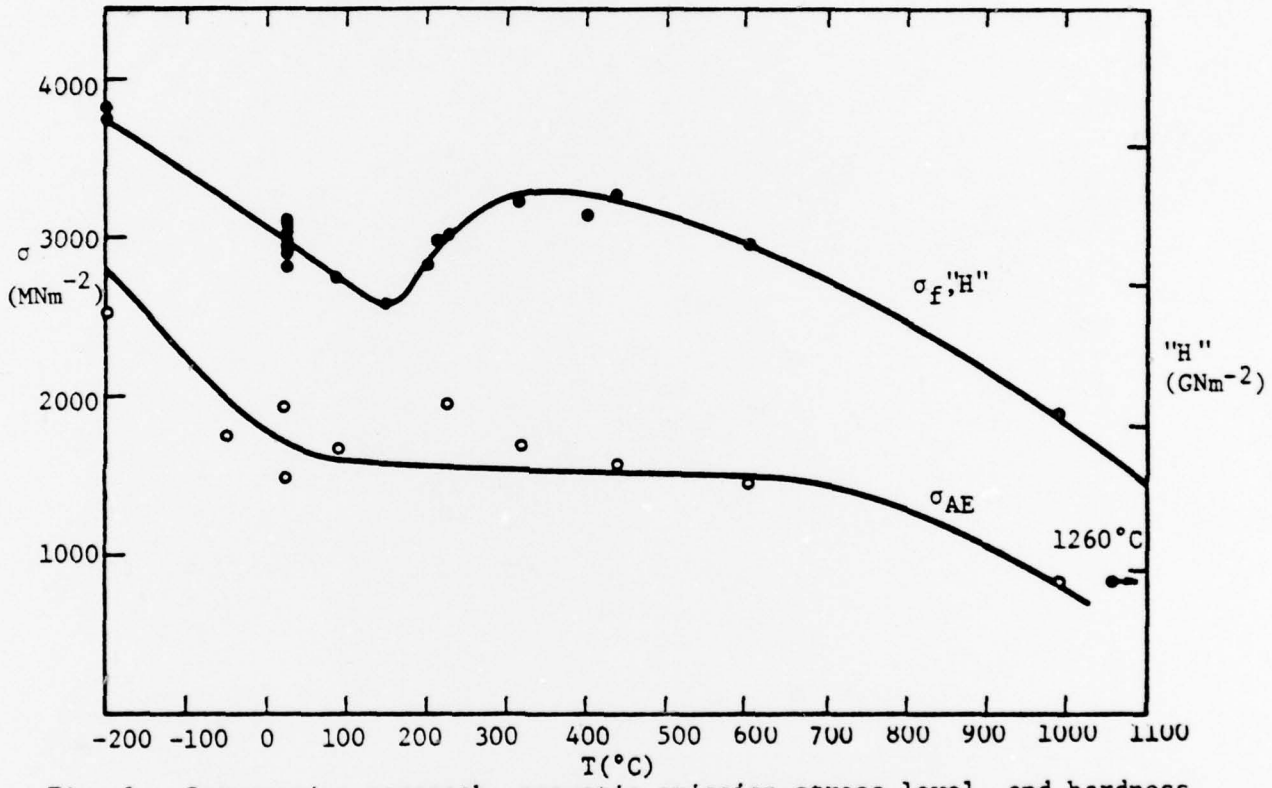

Fig. 1. Compressive strength, acoustic emission stress level, and hardness, versus temperature for Al_2O_3.

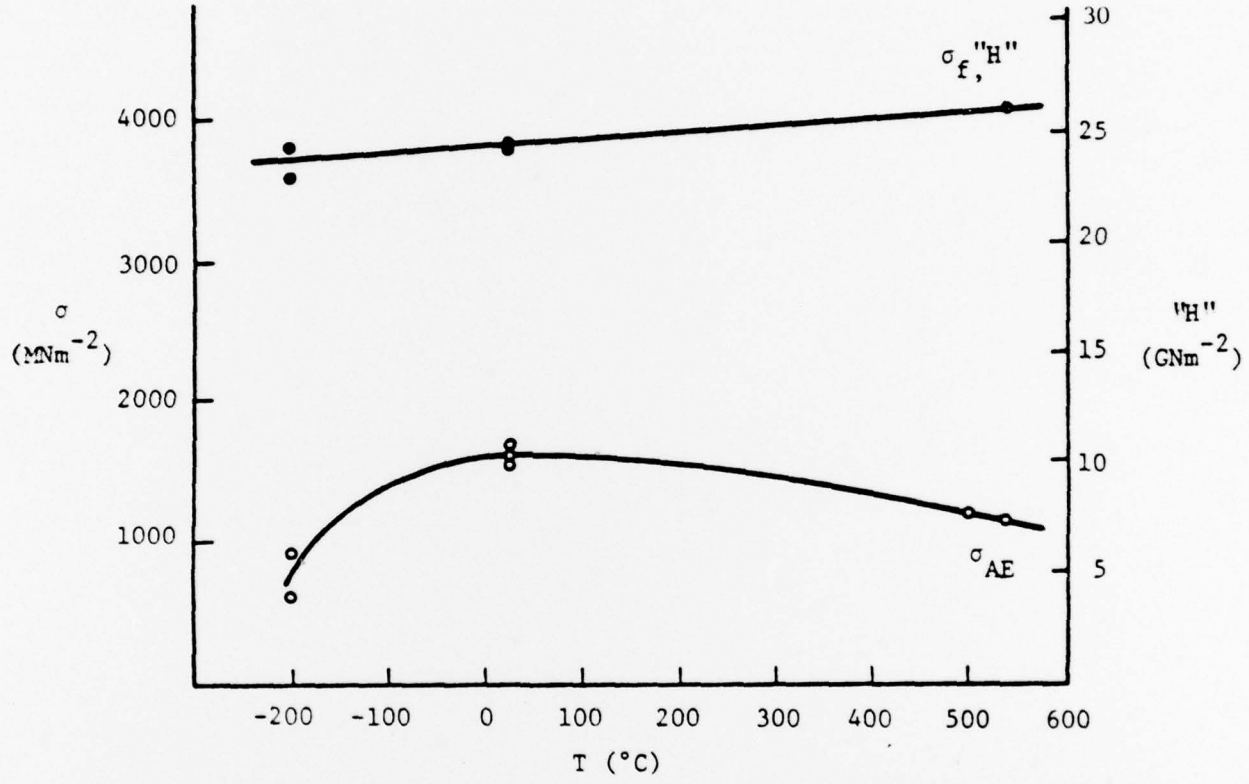

Fig. 2. Compressive strength acoustic emission stress level, and hardness versus temperature for α-SiC.

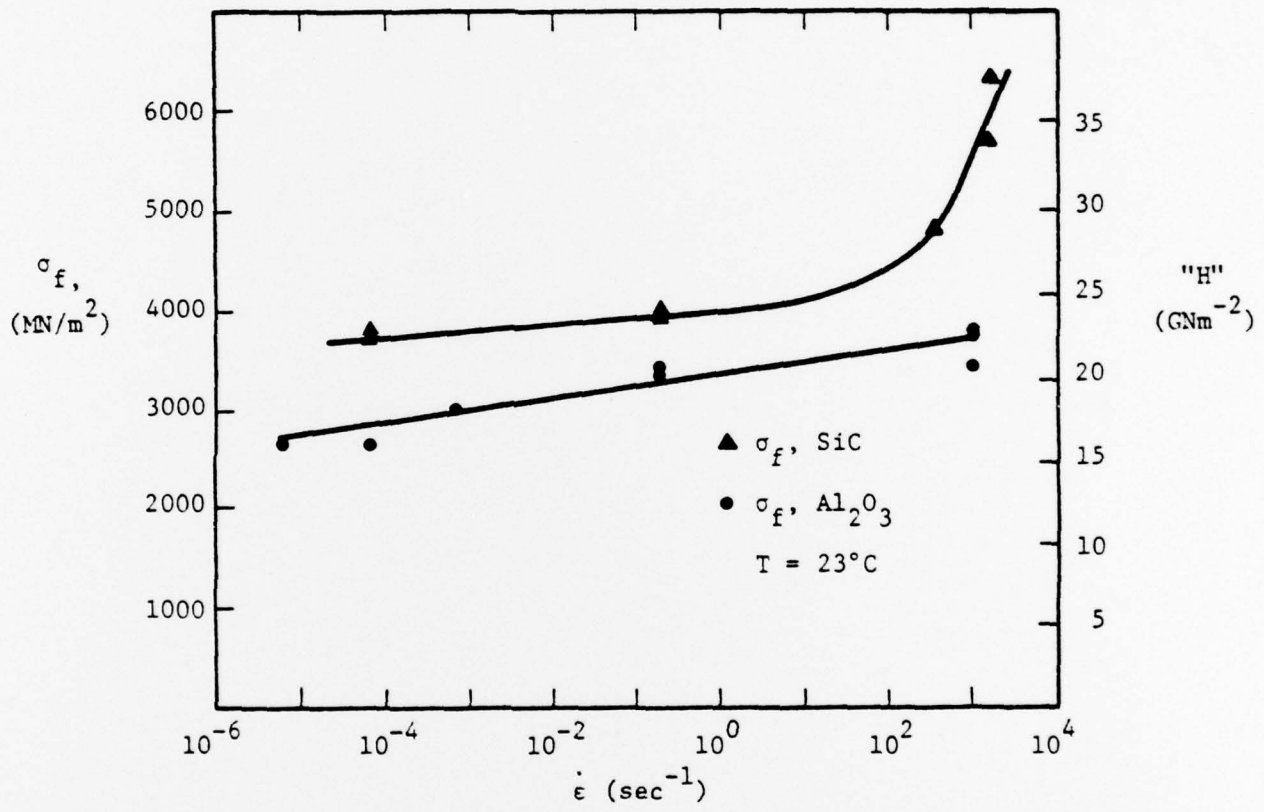

Fig. 3 Compressive strength and hardness versus strain rate for Al_2O_3 and SiC at T = 23°C.

DISCUSSION

Tensile Lifetimes Following Compressive Loading

It is clear that compressive loads well below the compressive failure level may nevertheless introduce damage. The significance of the damage during subsequent static tensile loading depends on the size of the flaws, their orientation relative to the tensile field, temperature, loading rate, and environment. It is instructive to consider a few cases based on the preceding results.

Based on a typical compressive crack, in Lucalox, of length 55 μm, one can calculate the stress intensity in a subsequent tensile field according to

$$K_I = k \sqrt{a}\, \sigma \qquad (1)$$

where a conservative value for k is about 1.4. Assuming an operating tensile stress level of, say, 200 MNm^{-2}, then $K_I = 1.6 MNm^{-3/2}$. If one then considers slow crack velocity V versus K_I data for Lucalox(Fig. 4), it is apparent that at lower temperatures, the specified operating conditions are safe for the given set of compression induced flaws. At 1300°C, however, V would be nearly a micron per second. Since K_{IC} at this temperature is only ~$2.4 MNm^{-3/2}$, meaning a critical flaw size a_c of 75μm, the specimen would have only seconds to live. It is clear that at high temperatures, cracks of the size introduced during compression would act to reduce permissible operating stress levels in Lucalox; 200 MNm^{-2} is well below the moninal failure stress at 1300°C.

Similar considerations can be seen to hold for Sic, if it can be assumed that V-K_I for hot-pressed SiC (Fig. 5) is equivalent to that for the sintered

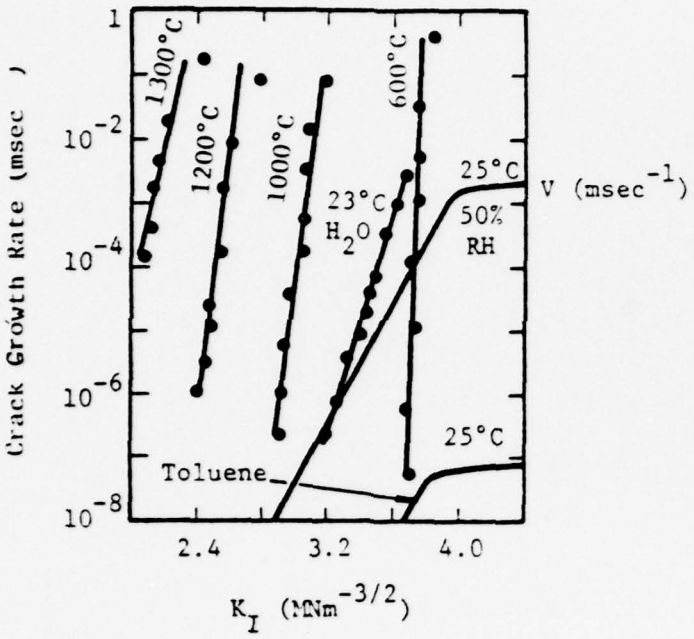

Fig. 4. Slow crack velocity versus stress intensity factor for Lucalox Al_2O_3, various temperatures and environments. Data from Evans (1973), Evans, Linzer, and Russell (1974) and Williams and Evans (1973).

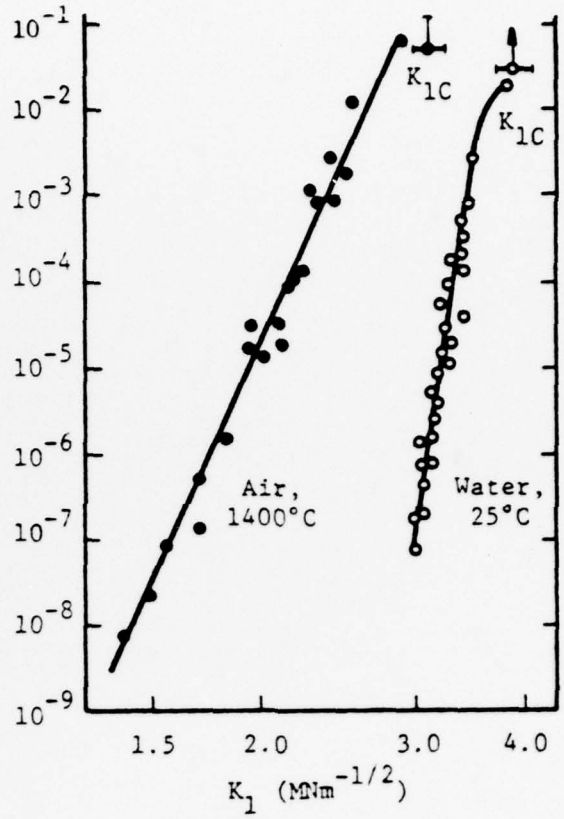

Fig. 5. Slow crack velocity versus stress intensity factor for hot-pressed SiC (Evans and Lange, 1975).

material. For an initial compressive crack of length 20μm, suppose a tensile operating stress of 350 MNm^{-2} (due to the higher strength in general of SiC). This yields $K_I = 1.55 MNm^{-3/2}$ which, on the basis of Fig. 5, with $T = 1400^oC$, corresponds to V = 0.1μm/sec. This predicts at least a finite (but still very short) lifetime, since for α-SiC, K_{1C} at $T = 1400^oC$ is approximately $7MNm^{-3/2}$, or a crack length of ~250μm. Again it would seem that the tensile operating stress level would be compromised, since 350 MNm^{-2} is only about 60% of the nominal tensile strength at 1400^oC.

Effect of Compressive Strength (Hardness) On Indentation Fracture

Particle impacts can cause two principal kinds ofdamage: (1) erosion, i.e., volume loss, through lateral cracking, and (2) strength degradation, through radial or median crack nucleation. With regard to the former, Evans, Gulden, and Rosenblatt (1978) have shown that the amount of material removed per particle impact $\bar{V}_i$ is given by

$$\bar{V}_i \propto V_o^{2.5} R_p^{4} \rho_P^{0.3} H^{-0.3} K_c^{1.5} \qquad (2)$$

where V_o is the particle velocity, R_p the particle radius, and ρ_p the particle density. In our treatment, we shall hold these factors constant, and consider only the effect of H and K_c.

Similarly, Lawn and Evans (1977) have shown that during indentation, the threshold crack size

$$C^* \propto \left(\frac{K_c}{H}\right)^2 \qquad (3)$$

and is produced by a threshold load

$$P^* \propto \left(\frac{K_c}{H}\right)^3 K_c \qquad (4)$$

We now utilize the temperature dependent hardness results of Figs. 1 and 2 and the dynamic hardness data of Fig. 3, together with measurements (by others, Fig. 6) of the temperature dependence of K_{1C} for sintered α-SiC and Lucalox Al_2O_3, in evaluating the T, $\dot{\varepsilon}$ sensitivity of $\bar{V}_i$, C*, and P*. No data exists, to the authors' knowledge, of K_{1C} ($\dot{\varepsilon}$) for either material; however, Evans and Wilshaw (1977) state that for ceramics K_{1C} is "generally similar" to the dynamic fracture toughness K_D. We therefore will assume $K_{1C} = K_D$. In addition, we will assume that $\sigma_f(T)$ for α-SiC at higher temperatures than those already tested is simply an extension of the current plot (Fig. 2), as is the case for tensile failure (Kraft and Dooher, 1976).

These data are used to calculate, for α-SiC and Lucalox, the quantities $\bar{V}_i/\bar{V}_{io}$, C^*/C^*_o , and P^*/P^*_o as functions of T and $\dot{\varepsilon}$, where $\bar{V}_{io}$, C^*_o, and P^*_o are simply the values of Equations (2), (3), and (4) for T = 23°C, $\dot{\varepsilon} = 7 \times 10^{-5}\,sec^{-1}$. The results are summarized in Figs. 7 to 11.

Temperature has a large effect on C*, P*, and $\bar{V}_i$. In Fig. 7, the large increase in C* is caused by the rapid dropoff in H; this is counteracted by the increase, Fig. 8, in P* due to the fact that K_{1C} does not decrease as rapidly as H, and in addition, enters through the fourth power rather than the third, as for H. Although the increases in C* and P* are not as spectacular as those for Al_2O_3, they still are sizeable; P* at 1600°C is four times that at room temperature. It is interesting to note that for Al_2O_3, $\bar{V}_i$ increases by a factor of nearly eight from 23° to 1400°C, (Fig. 9), while over the same range, the removal rate for SiC decreases by nearly 50%.

Increases in strain rate (impact velocity) cause the same effect, a steady decrease, upon C*, P*, and $\bar{V}_i$ in both materials. As shown in Fig. 10,

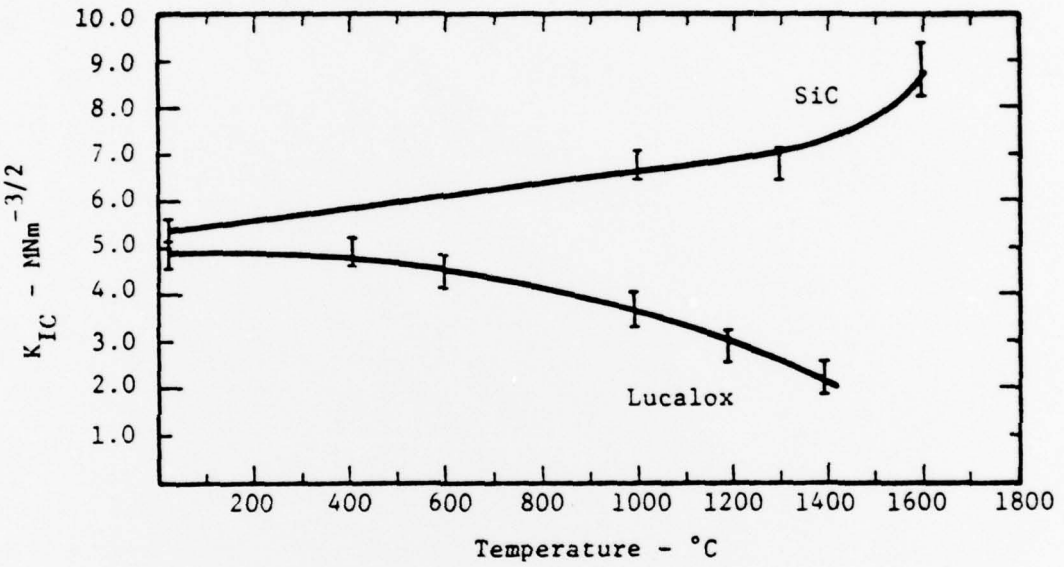

Fig. 6. Fracture toughness versus temperature for α-SiC (Kraft and Dooher, 1976) and Lucalox Al_2O_3 (Evans, Linzer, and Russell, 1974).

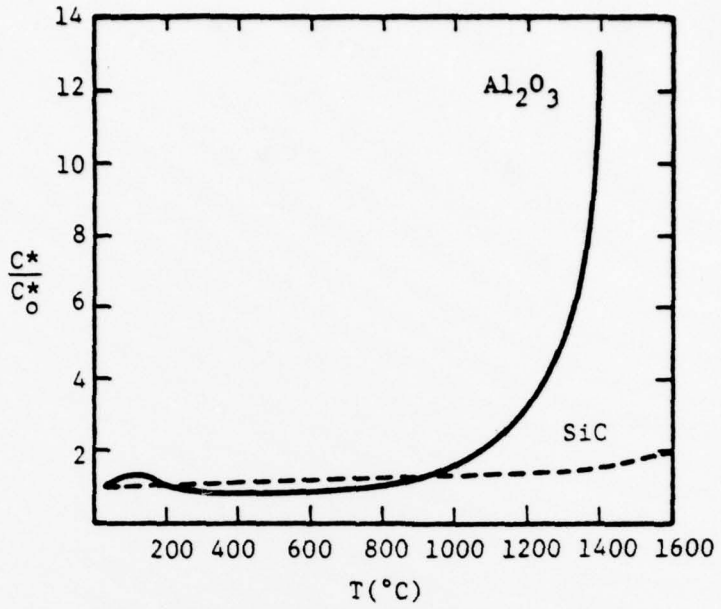

Fig. 7. Threshold crack size versus temperature during quasistatic indentation.

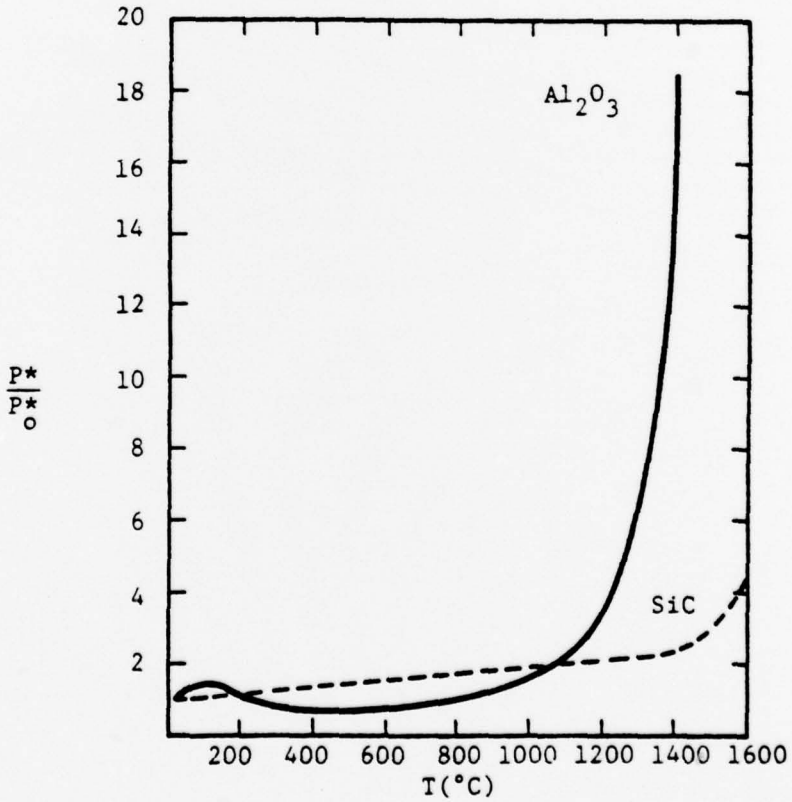

Fig. 8. Threshold load versus temperature during quasistatic indentation.

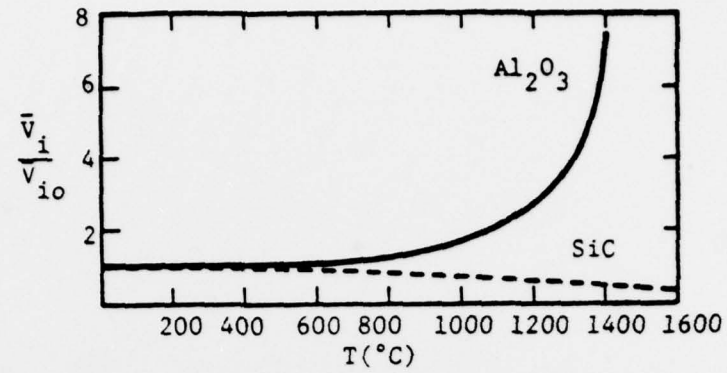

Fig. 9. Material volume removed versus temperature during quasistatic impact.

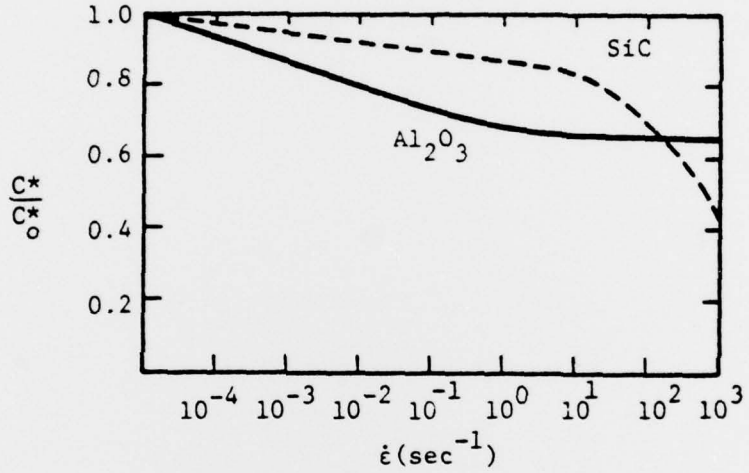

Fig. 10. Threshold crack size versus strain rate during dynamic indentation at 23°C.

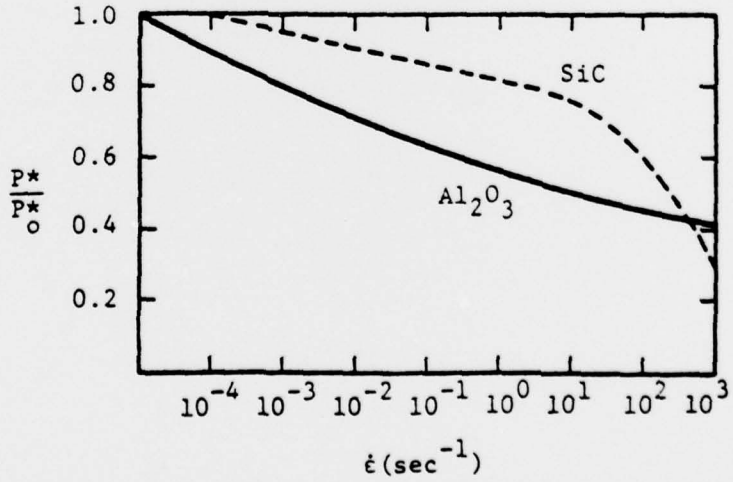

Fig. 11. Threshold load versus strain rate during dynamic indentation at 23°C.

the threshold crack size decreases with increasing $\dot{\varepsilon}$ most rapidly in Al_2O_3, while the net decrease is greatest for the SiC. Unfortunately, these beneficial effects are counteracted by corresponding decreases in the minimum load required to nucleate the cracks (Fig. 11). No plot is shown for $\bar{V}_i$ versus $\dot{\varepsilon}$, since the dependence was not strong; however, recent unpublished results indicate that strain rate may have a significant dependence upon $\bar{V}_i$ at higher temperature.

CONCLUSIONS

It is clear from the foregoing results that if the relationship between "H" and σ_f is as assumed, profound alterations may be affected by $\dot{\varepsilon}$ and T in the tensile and indentation/impact characteristics of strong ceramics. Because of the fashion in which they are incorporated into the indentation relationships in particular, T are $\dot{\varepsilon}$-induced hardness changes may exert significantly out-of-proportion influence.

At present, the predicted results must be treated with caution, because of the assumptions involved. Critical experiments remain to be carried out: (1) actual hardness as a function of T and $\dot{\varepsilon}$, especially where both T and $\dot{\varepsilon}$ are high, simulating high velocity impact of a hot target; (2) actual measurement of threshold crack size and load as a function of T and $\dot{\varepsilon}$; (3) K_c as a function of T within grains. Application of the "H" and K_c data used in the present work may suffer from the physical circumstances under which it was obtained, i.e., bulk compression tests, and standard fracture mechanics tests, in which grain boundary effects are important at high temperature. More relevant to the indentation/impact process would be micro-hardness tests within the interiors of grains, to determine both H and K_c at high temperature.

ACKNOWLEDGEMENTS

The authors are grateful for the support of the U.S. Office of Naval Research, Contract No. N00014-75-C-0668, during the course of this work.

REFERENCES

1. Evans, A.G. (1973). High-temperature slow crack growth in ceramic materials. In J.J. Burke, A.E. Gorum, and R.N. Katz (Eds.), Ceramics for High-Performance Applications, Brook Hill, Chestnut Hill, Mass. pp. 373-396.

2. Evans, A.G., Gulden, M.E., and Rosenblatt, M (1978). Impact damage in brittle materials in the elastic-plastic response regime. Proc. Roy. Soc. London, 361, 343-365.

3. Evans, A.G., and Lange, F.F. (1975). Crack propagation and fracture in silicon carbide. Jour. Mat. Sci., 10, 1659-1664.

4. Evans, A.G., Linzer, M., and Russell, L.R. (1974). Acoustic emission and crack propagation in polycrystalline alumina. Mat. Sci. Eng., 15, 253-261.

5. Evans, A.G., and Wilshaw, T.R. (1977). Dynamic solid particle damage in brittle materials: an appraisal. Jour. Mat. Sci., 12, 97-116.

6. Kraft, E.H., and Dooher, G.I. (1976). Mechanical response of high performance silicon carbides. Presented at Second International Conference on Mechanical Behavior of Materials, 16-20 August, 1976, Boston, Mass. (unpublished).

7. Lankford, J. (1977). Compressive strength and microplasticity in polycrystalline alumina. Jour. Mat. Sci., 12, 791-796.

8. Lankford, J. (1978). Tensile failure of unflawed polycrystalline Al_2O_3. Jour. Mat. Sci., 13, 351-357.

9. Lawn, B.R., and Evans, A.G. (1977). A model for crack initiation in elastic/plastic indentation fields. Jour. Mat. Sci., 12, 2195-2199.

10. Rice, R.W., (1970). The compressive strength of ceramics. In W.W. Kriegel and H. Palmour (Eds.), Ceramics in Severe Environments, Vol. 5, Plenum Press, New York, 195-229.

11. Williams, D.P., and Evans, A.G. (1973). A simple method for studying slow crack growth. Jour. Test. Eval., 1, 264-270.